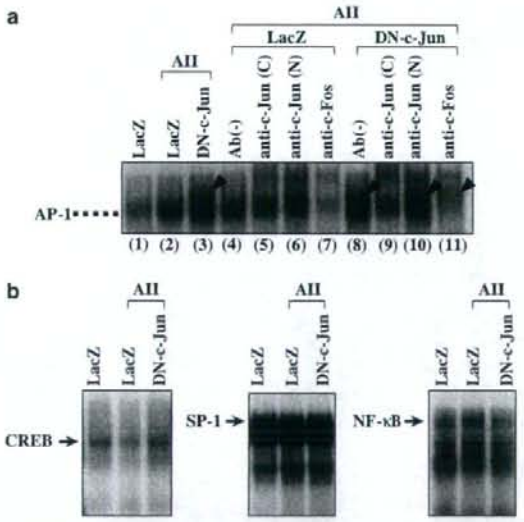

Figure 3 Gel mobility shift analysis of cardiac nuclear extract from angiotensin II (AngII)-infused rat subjected to *in vivo* cardiac gene transfer of DN-c-Jun or LacZ 2 days previously. (**a**) Endogeneous AP-1 is shown by dashed line. AngII infusion in rats significantly increased left ventricular endogeneous AP-1 DNA-binding activity (lanes (2) and (3)). LacZ did not affect AP-1 DNA-binding activity. As indicated by lane (3), DN-c-Jun gene transfer increased AP-1 DNA biding activity (indicated by the arrow). However, the position (the arrow) of AP-1 band due to DN-c-Jun shows the upper position to that of endogeneous AP-1 band (dashed line). This DN-c-Jun band was specific binding for AP-1, because the addition of unlabeled AP-1 oligonucleotide resulted in a decrease in the formation of AP-1 complexes in a dose-dependent manner while the addition of excess amounts of unlabeled mutant AP-1 oligonucleotide did not affect AP-1 complexes (data not shown). The lanes from (4) to (11) indicated supershift analysis from AngII-infused rats pretreated with LacZ or DN-c-Jun gene transfer. Endogenous AP-1 was supershifted with anti-c-Jun antibody recognizing the conserved DNA-binding domain of wild c-Jun (anti-c-Jun (C)) (lane 5), anti-c-Jun antibody recognizing the transactivation domain of wild c-Jun (anti-c-Jun (N)) (lane 6), or anti-c-Fos antibody (anti-c-Fos) (lane 7). While AP-1 DNA-binding activity, induced by DN-c-Jun, was supershifted by anti-c-Jun (C) (lane 9) but not with anti-c-Jun (N) (lane 10) or anti-c-Fos (lane 11). (**b**) *In vivo* cardiac gene transfer of DN-c-Jun did not apparently affect CREB, SP-1, or NF-κB-binding activity, thereby indicating the specific binding of transferred DN-c-Jun to AP-1 binding site.

anti-c-Jun antibody recognizing the conserved DNA-binding domain of wild c-Jun (anti-c-Jun(C)), anti-c-Jun antibody recognizing the transactivation domain of wild c-Jun (anti-c-Jun(N)), or anti-c-Fos antibody. On the other hand, as shown by gel mobility shift analysis of left ventricular nuclear proteins from DN-c-Jun-transduced rat, DN-c-Jun-induced AP-1 band was supershifted only with anti-c-Jun(C), but not with anti-c-Jun(N) or anti-c-Fos antibody. Furthermore, to confirm the specific binding of DN-c-Jun to AP-1 consensus sequence, we also examined the effect of Ad.DN-c-Jun on the CREB, SP-1 and NF-κB DNA-binding activity, by gel mobility shift assay. Ad.DN-c-Jun infection did not affect the CREB, SP-1 and NF-κB DNA-binding activity in LV, being consistent with our previous paper.[3]

Effects of DN-c-Jun gene transfer on angiotensin II-induced hypertension, and cardiac hypertrophy, p70S6 kinase and gene expressions

As shown in Figure 4(a), blood pressure of rats was significantly increased at 3 and 7 days after start of AngII infusion, compared with control rats subjected to saline infusion. No significant difference in blood pressure was noted between two groups of rats subjected to gene transfer of LacZ and DN-c-Jun, throughout AngII infusion. There was no significant difference in body weight among these three groups of rats at the end of the experiments.

AngII infusion for 7 days increased LV weight compared with control (2.52 ± 0.05 vs 1.94 ± 0.05 mg/g BW, $P < 0.01$), and this increase in LV weight was significantly suppressed by DN-c-Jun gene transfer (2.21 ± 0.05 mg/g BW, $P < 0.01$ (Figure 4(b)). LV phospho-p70S6 kinase levels were increased by AngII infusion by 1.3-fold ($P < 0.05$) and DN-c-Jun gene transfer significantly inhibited AngII-induced activation of LV p70S6 kinase ($P < 0.01$ (Figure 4(c)).

Figure 5 shows the effect of DN-c-Jun gene transfer on LV mRNA expressions related to cardiac hypertrophy and remodeling. LV mRNA levels for collagen I, III and IV, MCP-1, PAI-1 and BNP were elevated by AngII infusion by 1.6-, 1.5-, 1.5-, 1.8-, 2.4-, and 1.6-fold, respectively, and DN-c-Jun gene transfer significantly reduced all these mRNA levels. On the other hand, DN-c-Jun failed to suppress LV ANP mRNA expression, which were increased by AngII infusion by 5.4-fold. Interestingly, LV α-MHC mRNA expression, which was not altered by AngII infusion, was increased by DN-c-Jun gene transfer by 1.6-fold ($P < 0.05$).

Effects of DN-c-Jun gene transfer on blood pressure, and cardiac hypertrophy, p70S6kinase and gene expressions of hypertensive rats

As shown in Figure 6(a), there was no difference in blood pressure between LacZ group and DN-c-Jun group of SHRSP before cardiac gene transfer (162 ± 2 vs 163 ± 2 mmHg). DN-c-Jun transfer did not significantly affect blood pressure of SHRSP compared with control SHRSP at 7 and 14 days (177 ± 2 vs 177 ± 1 mmHg). LV weight corrected for body weight in DN-c-Jun group was smaller than that in control group (2.876 ± 0.034 vs 3.044 ± 0.052 mg/g BW, $P < 0.05$) (Figure 6(b)). LV phospho-p70S6 kinase levels in DN-c-Jun group was lower than those in control group ($P < 0.05$) (Figure 6(c)). Cardiac echocardiography in Figure 7 indicated that DN-c-Jun gene transfer significantly reduced LV anterior and posterior wall thickness of SHRSP ($P < 0.05$). The left ventricular weight, corrected for body weight, is significantly smaller in DN-c-Jun group than control group (2.68 ± 0.02 vs 2.77 ± 0.02 mg/g body weight; $P < 0.05$). As shown in Figure 8, compared with control group, DN-c-Jun gene transfer significantly reduced LV mRNA levels for collagen I, III and IV, MCP-1, and PAI-1 by 42, 41, 43, 32, and 61%, respectively. On the other hand, DN-c-Jun inversely elevated LV α-MHC mRNA levels by 2.8-fold. LV ANP BNP and β-MHC mRNA levels were not changed by DN-c-Jun, compared with control.

Discussion

Our present work provided the first evidence that *in vivo* blockade of c-Jun by the gene transfer technique

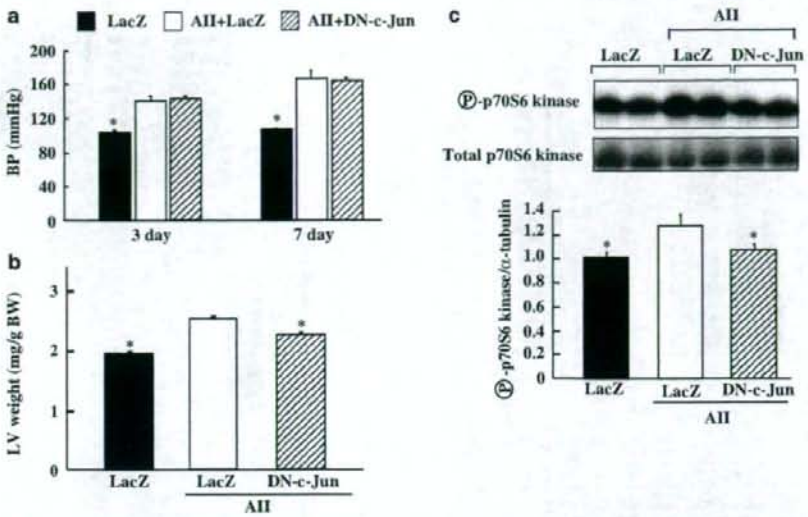

Figure 4 Effect of adenoviral DN-c-Jun on angiotensin II (AngII)-induced hypertension, and cardiac hypertrophy and p70S6 kinase phosphorylation. As shown in (**a**), cardiac gene transfer of DN-c-Jun did not affect hypertension induced by AngII. As shown in (**b**), AngII-induced increase in LV weight was significantly prevented by cardiac gene transfer of DN-c-Jun. As shown in (**c**), AngII-induced phophorylation of LV p70S6 kinase was significantly prevented by DN-c-Jun. Values are means ± s.e.m. ($n=7$ in each group). *$P<0.01$ vs AngII-infused group subjected to LacZ gene transfer (Control).

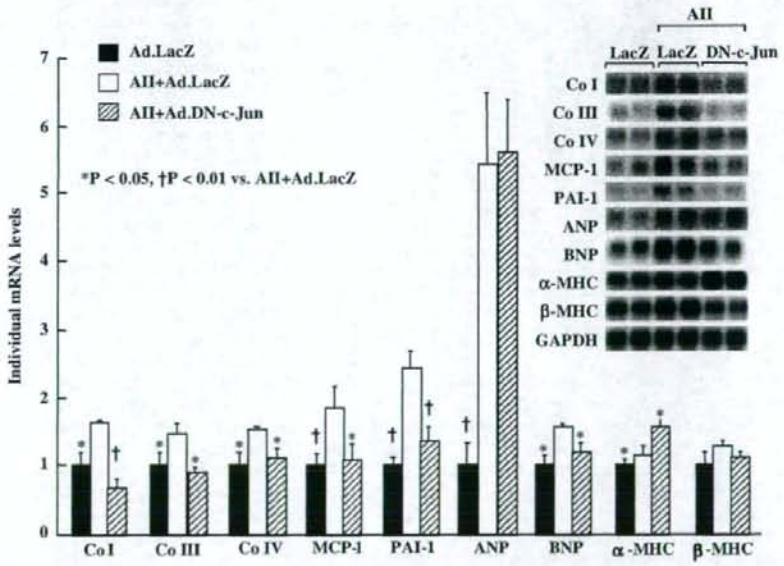

Figure 5 Effect of DN-c-Jun gene transfer on LV mRNA levels related to cardiac hypertrophy and remodeling in AngII-infused rats. Individual mRNA levels were corrected for GAPDH mRNA levels. Values are means ± s.e.m. ($n=7$ in each group). The mean value in control group (saline infusion) is expressed as 1.

suppressed cardiac hypertrophy and the gene expression of cardiac hypertrophic markers, induced by AngII infusion or hypertension. Thus, c-Jun seems to be involved in the molecular pathway responsible for pathologic cardiac hypertrophy.

Previous reports on *in vivo* experiments, by us and other groups of investigators, have showed that AngII is importantly involved in cardiac hypertrophy and remodeling, independently of blood pressure.[6,11,14,15] Moreover, AngII *in vivo* and *in vitro* induces the activation of

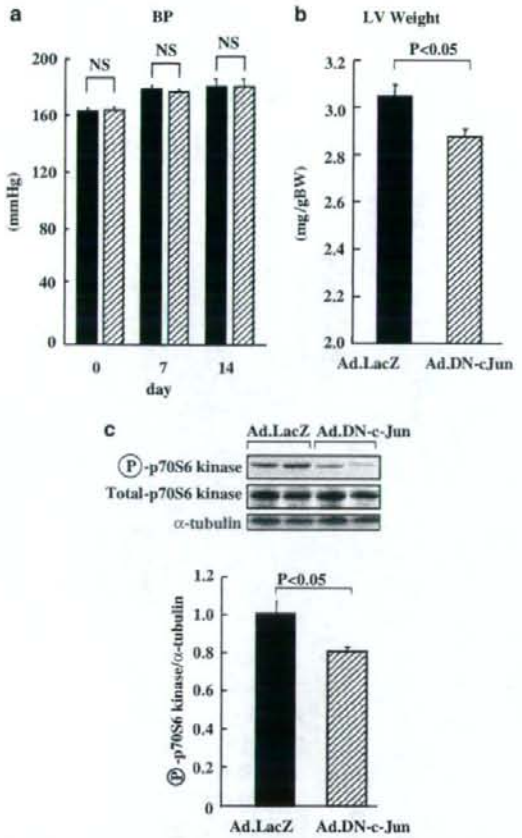

Figure 6 Effect of DN-c-Jun on blood pressure (BP), LV weight, and p70S6 kinase phosphorylation in SHRSP. (**a**) *In vivo* cardiac gene transfer of DN-c-Jun did not affect blood pressure of SHRSP throughout the experiment. (**b**) LV weight of SHRSP was significantly reduced at 14 days after *in vivo* cardiac gene transfer of DN-c-Jun. (**c**) Phosphorylation of p70S6 kinase in LV of SHRSP was significantly reduced at 14 days after DN-c-Jun gene transfer. Values are means ± s.e.m. ($n = 7$ in each group). NS, not significant.

AP-1 related to c-Jun in cardiomyocytes.[4] However, the molecular mechanism responsible for AngII-induced cardiac hypertrophy *in vivo* remains to be determined. There is no available report on the effect of c-Jun inhibition on cardiac hypertrophy *in vivo*, which encouraged us to examine the possible role of c-Jun in AngII-induced cardiac disease. To specifically inhibit cardiac c-Jun *in vivo*, we used gene transfer technique with adenoviral vector. The abundant expression of transferred gene in cardiac tissue by our technique, as shown in Figures 1–3, demonstrated the successful gene transfer technique employed in our work.

In the present experiments, we found that DN-c-Jun gene transfer significantly suppressed AngII-induced cardiac hypertrophy and gene expressions, despite no effect on blood pressure. These results demonstrate that c-Jun plays a critical role in AngII-induced cardiac disease. The suppression of cardiac hypertrophy by gene transfer of DN-c-Jun was accompanied by the inhibition

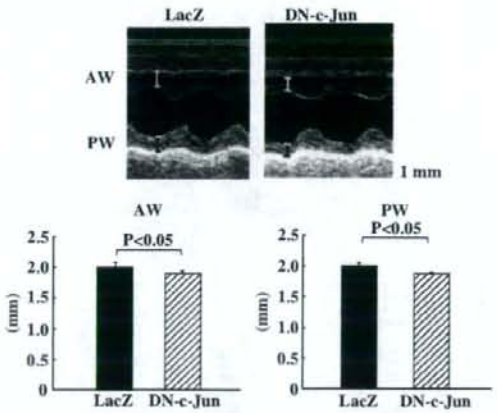

Figure 7 Echocardiography of SHRSP subjected to *in vivo* cardiac gene transfer of LacZ (control) or DN-c-Jun. As estimated by M-mode of echocardiography, anterior wall (AW) or posterior wall (PW) thickness of left ventricle in DN-c-Jun-transferred SHRSP was smaller than those of LacZ-transferred SHRSP. Values are means ± s.e.m. ($n = 7$ in each group). NS, not significant.

of p70S6 kinase phosphorylation. p70S6 kinase is a physiological kinase for the 40S ribosomal S6 protein and plays the critical role in protein synthesis.[16] Furthermore, p70S6 kinase phosphorylation is involved in AngII- or phenylephrine-induced cardiomyocyte hypertrophy *in vitro*[17,18] and is significantly activated in hypertensive heart.[19] Taken together with these findings, our observation suggests that p70S6 kinase may play some role in the prevention of AngII-induced cardiac hypertrophy by c-Jun blockade. However, further study is needed to elucidate our proposal.

In this study, AngII infusion caused the upregulation of cardiac mRNAs for collagen I, III and IV, ANP, BNP, MCP-1 and PAI-1, being in good agreement with our previous reports.[6] Of note are the observations that c-Jun blockade led to the inhibition of upregulation of the above-mentioned gene expressions except for ANP. Furthermore, c-Jun blockade caused the upregulation of α-MHC. These results demonstrated that c-Jun plays a pivotal role in AngII-mediated gene expression related to cardiac hypertrophy and remodeling.

To elucidate whether the important role of c-Jun in pathologic cardiac hypertrophy is limited to AngII-mediated cardiac hypertrophy or not, we also investigated the effect of DN-c-Jun on cardiac hypertrophy in SHRSP. SHRSP is the most popular model of genetic hypertension and is the very useful model of hypertensive cardiac hypertrophy and remodeling.[11,14,15,20] We have previously shown that SHRSP exhibits cardiac hypertrophy and upregulation of cardiac hypertrophy- and remodeling-associated gene expression, compared with normotensive rats.[11,15] Moreover, we have reported that cardiac AP1 activity related to c-Jun is significantly increased in SHRSP compared with normotensive rats.[21] In this study, as in the case of AngII-infused rats as described above, cardiac gene transfer of DN-c-Jun in SHRSP regressed cardiac hypertrophy and reduced p70S6 kinase phosphorylation. Moreover, DN-c-Jun gene transfer suppressed the upregulation of cardiac collagen I, III and IV, MCP-1 and PAI-1 in SHRSP, being in

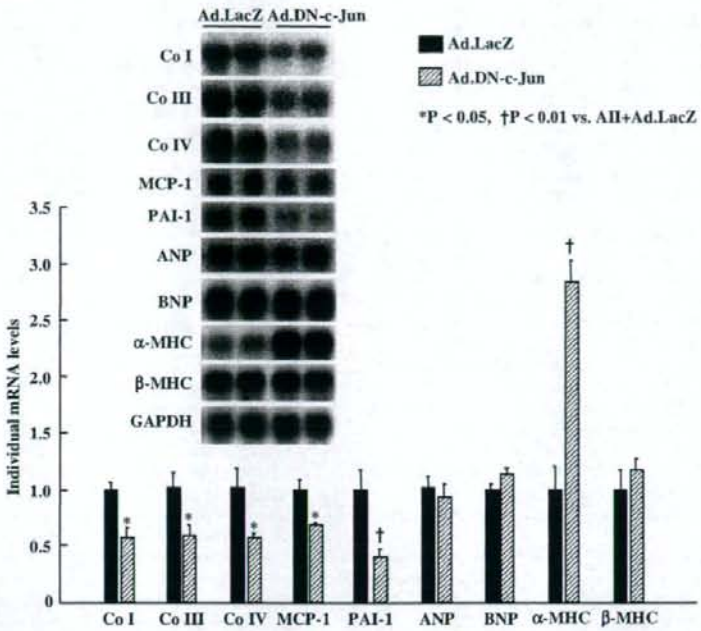

Figure 8 Effect of DN-c-Jun on LV mRNA levels related to cardiac hypertrophy and remodeling in SHRSP. Individual mRNA levels were corrected for GAPDH mRNA levels. Values are means ± s.e.m. ($n = 7$ in each group). The mean value in control group (LacZ gene transfer) is expressed as 1.

consistent with the case of AngII-infused rats. These observations demonstrated that c-Jun participated in cardiac hypertrophy and gene expressions in SHRSP. Thus, c-Jun is the critical molecule of cardiac hypertrophy and gene reprogramming induced not only by AngII but also by hypertension. However, differing from the case of AngII infusion, DN-c-Jun failed to suppress cardiac BNP in SHRSP. The present work did not allow us to elucidate the reason for the difference in BNP expression, although it suggested that c-Jun might play a minor role in cardiac BNP expression in SHRSP.

In this study, as well as AngII-infused rats, DN-c-Jun upregulated cardiac α-MHC mRNA without affecting β-MHC in SHRSP. Cardiac contractile proteins, including α-MHC and β-MHC, play a crucial role in the modulation of cardiac performance.[22,23] α-MHC, which has higher Ca^{2+}- and actin-activated ATPase activity, is associated with an increased shortening velocity of the cardiac fibers, whereas β-MHC, which has lower ATPase activity, is associated with slower shortening velocity.[22,23] Therefore, the alteration of ratio of α-MHC to β-MHC significantly affects cardiac performance. Collectively, our present results suggest that c-Jun may be implicated in the regulation of cardiac contractile protein, although further study is needed to elucidate our assumption.

In conclusion, our present experimental observations support the notion that c-Jun is implicated in pathologic cardiac hypertrophy and delivery of DN-c-Jun may have some utility for treatment of cardiac hypertrophy. However, the clinical application of DN-c-Jun is hampered by the short-lived nature of adenovirus expression and inherent problems with immune recognition and reaction. Therefore, the technical development of gene delivery to the heart is essential to elucidate the significance of DN-c-Jun delivery in cardiac disease.

Acknowledgements

This work was supported in part by a Grant-in-Aid for Scientific Research from the Ministry of Education, Science, Sports and Culture (14370036 and 14570083), and Hoh-ansha Foundation.

References

1 Leppa S, Bohmann D. Diverse functions of JNK signaling and c-Jun in stress response and apoptosis. *Oncogene* 1999; **18**: 6158–6162.
2 Yasumoto H, Kim S, Zhan Y, Miyazaki H, Hoshiga M, Kaneda Y *et al*. Dominant negative c-jun gene transfer inhibits vascular smooth muscle cell proliferation and neointimal hyperplasia in rats. *Gene Therapy* 2001; **8**: 1682–1689.
3 Zhan Y, Kim S, Yasumoto H, Namba M, Miyazaki H, Iwao H. Effects of dominant-negative c-Jun on platelet-derived growth factor-induced vascular smooth muscle cell proliferation. *Arterioscler Thromb Vasc Biol* 2002; **22**: 82–88.
4 Yano M, Kim S, Izumi Y, Yamanaka S, Iwao H. Differential activation of cardiac c-jun amino-terminal kinase and extracellular signal-regulated kinase in angiotensin II-mediated hypertension. *Circ Res* 1998; **83**: 752–760.
5 Izumi Y, Kim S, Murakami T, Yamanaka S, Iwao H. Cardiac mitogen-activated protein kinase activities are chronically increased in stroke-prone hypertensive rats. *Hypertension* 1998; **31**: 50–56.

6 Kim S, Ohta K, Hamaguchi A, Yukimura T, Miura K, Iwao H. Angiotensin II induces cardiac phenotypic modulation and remodeling *in vivo* in rats. *Hypertension* 1995; **25**: 1252–1259.
7 Brown PH, Chen TK, Birrer MJ. Mechanism of action of a dominant-negative mutant of c-Jun. *Oncogene* 1994; **9**: 791–799.
8 Miyake S, Makimura M, Kanegae Y, Harada S, Sato Y, Takamori K *et al*. Efficient generation of recombinant adenoviruses using adenovirus DNA-terminal protein complex and a cosmid bearing the full-length virus genome. *Proc Natl Acad Sci USA* 1996; **93**: 1320–1324.
9 Xu ZL, Mizuguchi H, Mayumi T, Hayakawa T. Regulated gene expression from adenovirus vectors: a systematic comparison of various inducible systems. *Gene* 2003; **309**: 145–151.
10 Hajjar RJ, Schmidt U, Matsui T, Guerrero JL, Lee KH, Gwathmey JK *et al*. Modulation of ventricular function through gene transfer *in vivo*. *Proc Natl Acad Sci USA* 1998; **95**: 5251–5256.
11 Kim S, Ohta K, Hamaguchi A, Omura T, Yukimura T, Miura K *et al*. Angiotensin II type I receptor antagonist inhibits the gene expression of transforming growth factor-beta 1 and extracellular matrix in cardiac and vascular tissues of hypertensive rats. *J Pharmacol Exp Ther* 1995; **273**: 509–515.
12 Suto R, Tominaga K, Mizuguchi H, Sasaki E, Higuchi K, Kim S *et al*. Dominant-negative mutant of c-Jun gene transfer: a novel therapeutic strategy for colorectal cancer. *Gene Therapy* 2004; **11**: 187–193.
13 Omura T, Yoshiyama M, Yoshida K, Nakamura Y, Kim S, Iwao H *et al*. Dominant negative mutant of c-Jun inhibits cardiomyocyte hypertrophy induced by endothelin 1 and phenylephrine. *Hypertension* 2002; **39**: 81–86.
14 Kim S, Iwao H. Molecular and cellular mechanisms of angiotensin II-mediated cardiovascular and renal diseases. *Pharmacol Rev* 2000; **52**: 11–34.
15 Kim S, Ohta K, Hamaguchi A, Yukimura T, Miura K, Iwao H. Effects of an AT1 receptor antagonist, an ACE inhibitor and a calcium channel antagonist on cardiac gene expressions in hypertensive rats. *Br J Pharmacol* 1996; **118**: 549–556.
16 Schmelzle T, Hall MN. TOR, a central controller of cell growth. *Cell* 2000; **103**: 253–262.
17 Boluyt MO, Zheng JS, Younes A, Long X, O'Neill L, Silverman H *et al*. Rapamycin inhibits alpha 1-adrenergic receptor-stimulated cardiac myocyte hypertrophy but not activation of hypertrophy-associated genes. Evidence for involvement of p70 S6 kinase. *Circ Res* 1997; **81**: 176–186.
18 Sadoshima J, Izumo S. Rapamycin selectively inhibits angiotensin II-induced increase in protein synthesis in cardiac myocytes *in vitro*. Potential role of 70-kD S6 kinase in angiotensin II-induced cardiac hypertrophy. *Circ Res* 1995; **77**: 1040–1052.
19 Shioi T, McMullen JR, Tarnavski O, Converso K, Sherwood MC, Manning WJ *et al*. Rapamycin attenuates load-induced cardiac hypertrophy in mice. *Circulation* 2003; **107**: 1664–1670.
20 Kim S, Zhan Y, Izumi Y, Iwao H. Cardiovascular effects of combination of perindopril, candesartan, and amlodipine in hypertensive rats. *Hypertension* 2000; **35**: 769–774.
21 Izumi Y, Kim S, Zhan Y, Namba M, Yasumoto H, Iwao H. Important role of angiotensin II-mediated c-Jun NH(2)-terminal kinase activation in cardiac hypertrophy in hypertensive rats. *Hypertension* 2000; **36**: 511–516.
22 Nadal-Ginard B, Mahdavi V. Molecular basis of cardiac performance. Plasticity of the myocardium generated through protein isoform switches. *J Clin Invest* 1989; **84**: 1693–1700.
23 Parker TG, Schneider MD. Growth factors, proto-oncogenes, and plasticity of the cardiac phenotype. *Annu Rev Physiol* 1991; **53**: 179–200.

Downloaded from heart.bmj.com on 29 March 2009

BASIC RESEARCH

Microbubble destruction with ultrasound augments neovascularisation by bone marrow cell transplantation in rat hind limb ischaemia

S Enomoto, M Yoshiyama, T Omura, R Matsumoto, T Kusuyama, D Nishiya, Y Izumi, K Akioka, H Iwao, K Takeuchi, J Yoshikawa

Heart 2006;**92**:515–520. doi: 10.1136/hrt.2005.064162

See end of article for authors' affiliations

Correspondence to: Dr Takashi Omura, Department of Internal Medicine and Cardiology, Osaka City University Medical School, 1-4-3 Asahimachi, Abeno-ku, Osaka 545-8585, Japan; omura@med.osaka-cu.ac.jp

Accepted 30 June 2005
Published Online First 1 July 2005

Objective: To examine the effects of microbubble destruction with ultrasound (MB) combined with bone marrow derived mononuclear cell transplantation (BMT) into ischaemic tissues in rat hind limb ischaemia.
Methods and results: Unilateral hind limb ischaemia was surgically induced in Lewis rats. At postoperative day 7, rats were randomly divided into three groups: a vehicle treated group, an ultrasound treated group, and an MB treated group. MB treatment increased vascular endothelial growth factor mRNA as assessed by real time polymerase chain reaction (3.0-fold, $p < 0.05$). At four weeks, the MB group had increases in laser Doppler blood flow index (LDBFI; 1.2-fold, $p < 0.05$), angiographically detectable collateral vessels (angiographic score: 1.4-fold, $p < 0.01$), and capillary to muscle fibre ratio (1.4-fold, $p < 0.01$) in ischaemic limbs compared with the vehicle treated group. No differences were seen between the vehicle and ultrasound treated groups. Secondly, rats were allocated to vehicle treatment, BMT (5×10^6 cells/rat), or a combination of MB and BMT (MB+BMT) at seven days after hind limb ischaemia. BMT treatment significantly increased LDBFI, angiographic score, and capillary to muscle fibre ratio compared with vehicle treatment. Interestingly, MB+BMT treatment produced significantly greater LDBFI (1.2-fold, $p < 0.01$), angiographic score (1.5-fold, $p < 0.01$), and capillary to muscle fibre ratio (1.5-fold, $p < 0.05$) than BMT treatment alone.
Conclusions: MB may be a useful technique to enhance BMT induced neovascularisation.

Recently, investigators have begun to test the feasibility of using microbubbles for therapeutic purposes, primarily as targeted gene delivery systems.[1 2] These studies illustrate the promise of ultrasound–microbubble based therapeutics. Other studies have shown that the application of low frequency ultrasound to intravascular microbubble contrast agents creates small capillary ruptures.[3 4] Song *et al*[3] found that capillary rupture elicited by destruction of ultrasonic contrast agent microbubbles with 1 MHz ultrasound stimulated arteriolar remodelling in skeletal muscle. This remodelling response caused an increase in nutrient blood flow two weeks after treatment. Therefore, this technique may have the potential for restoring nutrient blood flow to skeletal muscle. However, the ultrasound–microbubble treatment was applied to normal rather than ischaemic hind limbs.

Endothelial progenitor cells (EPCs) have been found to participate in postnatal neovascularisation after mobilisation from bone marrow.[5] Previous studies have shown that bone marrow mononuclear cells (BM-MNCs) contain not only EPCs but also angiogenic factors and cytokines and that implantation of BM-MNCs into ischaemic tissues augments collateral vessel formation.[7 8] Several bone marrow subpopulations, such as EPCs and marrow derived stromal cells, may be able to differentiate into one or more of the cellular components of the vascular bed.[6 9] Kinnaird *et al*[10] showed that marrow derived stromal cells secrete a wide array of arteriogenic cytokines and can contribute to collateral remodelling through paracrine mechanisms. These studies suggested that BM-MNC transplantation (BMT) may be a useful strategy for therapeutic neovascularisation in ischaemic tissues in adults. However, techniques for enhancing BMT induced neovascularisation have not been well developed.

In the present study, we examined whether microbubble destruction with ultrasound (MB) augments neovascularisation in rat hind limb ischaemia and the effectiveness of microbubble treatment combined with BMT.

METHODS

Unilateral hind limb ischaemia and ultrasound application

The rat ischaemic hind limb model is a modification of a two stage procedure previously described.[11] Ischaemia was created in the left hind limb of inbred male Lewis rats (SLC, Shizuoka, Japan) under anaesthesia with sodium pentobarbital (50 mg/kg intraperitoneally). All left side branches of the aorta distal to the renal arteries and of the iliac artery were resected. On the same day as the second operation, the femoral artery was resected. In the first series of experiments, rats (n = 18) were subjected to unilateral hind limb ischaemia. At postoperative day 7, the control group (n = 6) and the second group (n = 6; ultrasound group) received a bolus intravenous injection of 0.3 ml saline through the jugular vein. The third group (n = 6; MB group) received a bolus intravenous injection of microbubble solution (0.3 ml of Optison; Nepa Gene Co Ltd, Chiba, Japan) in the same manner. Ten seconds after microbubble (or saline) injection, ultrasound treatment was applied to the ultrasound and MB groups with an ultrasound transducer (Sonitron 1000; Nepa Gene Co Ltd). A gracilis muscle was exposed to ultrasound for 10 minutes at 1 MHz, 2.0 W/cm^2

Abbreviations: BM-MNC, bone marrow mononuclear cells; BMT, bone marrow derived mononuclear cell transplantation; EPC, endothelial progenitor cell; LDBF, laser Doppler blood flow; LDBFI, laser Doppler blood flow index; MB, microbubble destruction with ultrasound; PCR, polymerase chain reaction; VEGF, vascular endothelial growth factor

Downloaded from heart.bmj.com on 29 March 2009

output intensity (corresponding to a mechanical index of 0.2), and 50% duty cycle. In the preliminary examination, acoustic destruction of microbubbles in the ischaemic hind limb was observed with an intravital charge coupled device camera microscope (RM-0001; Nihon Kohden, Tokyo, Japan). Microbubble (or saline) infusion and ultrasound treatment were applied three times a week until postoperative day 28.

Laser Doppler analysis and angiography

We measured the ratio of the ischaemic (left) to the normal (right) limb blood flow with a laser Doppler blood flow (LDBF) image analyser (Moor Instruments, Axminster, UK) as described previously.[12] Before laser scanning was initiated, rats were placed on a heating plate kept at 37°C to minimise data variations due to body temperature. After blood flow was scanned twice, stored images were quantified by computer and the average flows of ischaemic and non-ischaemic limbs were calculated (moorLDI Image Processing version 3.08; Moor Instruments). To minimise variation due to ambient light and temperature, the LDBF index (LDBFI) was expressed as the ratio of ischaemic to non-ischaemic limb blood flow. The interobserver and intraobserver variabilities of LDBFI are 5.7% and 3.5%, respectively. Collateral formation was evaluated by using a Microfocus *x* ray television device (Hitex Co Ltd, Osaka, Japan) on day 28. A catheter was inserted through the right femoral artery and advanced to the lower abdominal aorta. Angiograms were taken two seconds after the injection of 0.5 ml contrast medium (Iopamiron; Schering). To quantitatively assess the extent of collateral vessel formation, we calculated the angiographic score as described previously.[13] The interobserver and intraobserver variabilities of the angiographic score are 6.3% and 4.5%, respectively.

Histological analysis

At day 30 (23 days after treatment), rats were killed with an overdose of pentobarbital. Four pieces of ischaemic tissue from the adductor and semimembranous muscles were obtained. Frozen sections were stained for alkaline phosphatase with an indoxyl-tetrazolium method to detect capillary endothelial cells as described previously.[13] Five fields from two muscle samples of each animal were randomly selected for capillary counts. To ensure that capillary densities were not overestimated as a consequence of myocyte atrophy or underestimated because of interstitial oedema, the capillary to muscle fibre ratio was determined. For immunohistochemical analysis of the inflammatory responses and angiogenic factor, leucocyte infiltration was examined by immunohistochemical staining of CD45, a common leucocyte antigen, and vascular endothelial growth factor (VEGF). Rats were killed two days after microbubble treatment. The

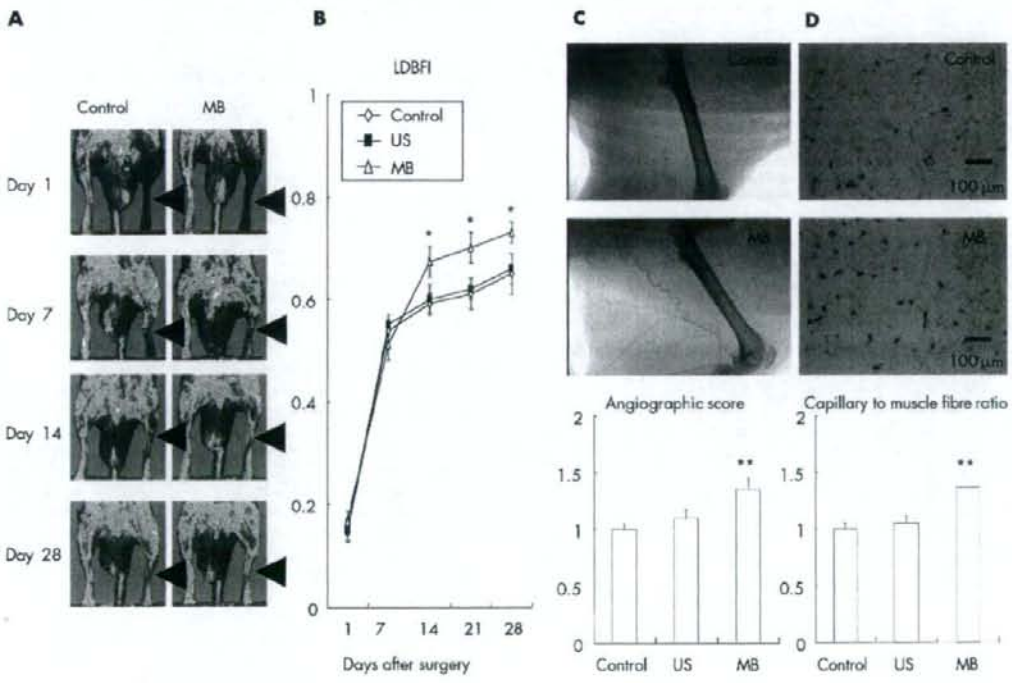

Figure 1 (A) Representative laser Doppler blood flow (LDBF) images. A low blood flow signal (dark blue) is observed in the ischaemic hind limb of the control group compared with a high blood flow signal (red to white) detected in the microbubble destruction with ultrasound (MB) group by LDBF. (B) Line graph of LDBF index (LDBFI) in each group. LDBFI was increased in the MB group compared with the control ($n = 6$ in each group). Ultrasound (US) alone did not change LDBFI compared with the control group. *$p < 0.05$ *v* control. (C) Representative angiograms obtained on postoperative day 28. Numerous collateral vessels were observed in the MB compared with the control. Angiographic score of ischaemic hind limbs was significantly greater in the MB group than in the control. **$p < 0.01$ *v* control. (D) Staining of ischaemic skeletal muscle tissues with alkaline phosphatase (dark blue) showing increased capillary counts in the MB group. Quantitative analysis showed significantly higher capillary to muscle fibre ratios in the MB group. **$p < 0.01$ *v* control.

Downloaded from heart.bmj.com on 29 March 2009

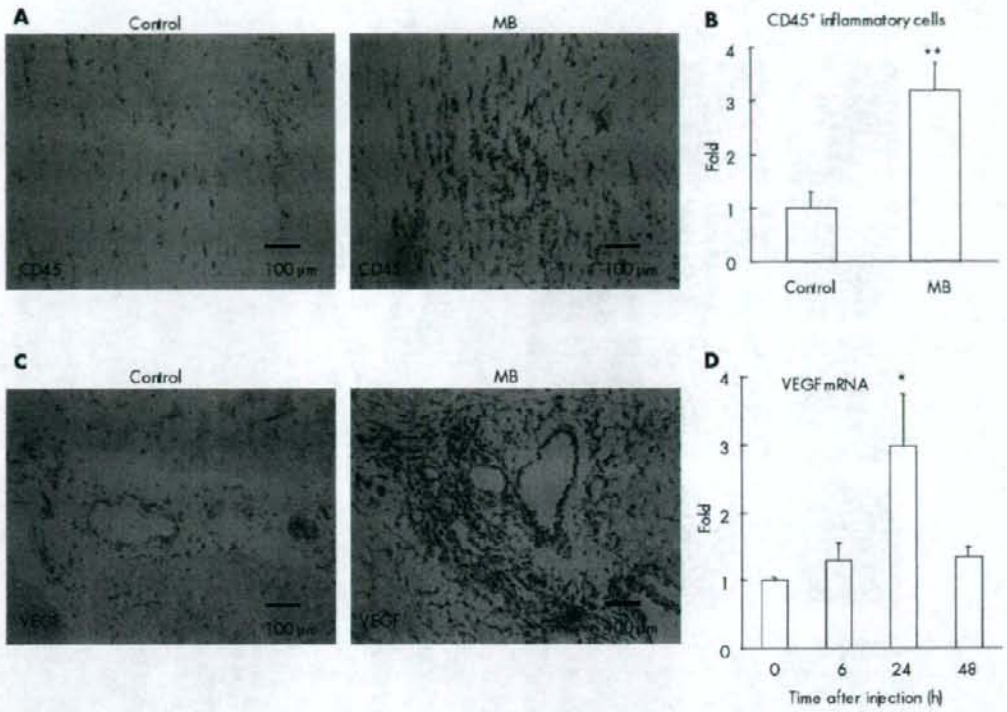

Figure 2 (A) Immunohistochemical staining for CD45 in ischaemic limbs 24 hours after US-microbubble treatment. Leucocyte infiltration was increased in the MB group compared with control. (B) Quantitative analysis showed increased CD45 positive inflammatory cell infiltration in the MB group compared with control. $^{**}p < 0.01$ *v* control. (C) Immunohistochemical staining for vascular endothelial growth factor (VEGF) in ischaemic limbs 48 hours after US-microbubble treatment. Perivascular grey-black label corresponds to VEGF expression. VEGF expression was increased in the MB group compared with control. (D) Quantitative real time reverse transcription and polymerase chain reaction analysis. Data were obtained from six independent ischaemic muscles for each time point and are expressed as mean (SEM) of mRNA normalised to glyceraldehyde-3-phosphate dehydrogenase. $^{*}p < 0.05$ *v* 0 hour.

ischaemic hind limbs were immediately embedded in optimal cutting compound (Tissue Tek, Miles Inc), frozen in dry ice-acetone, and cut into 5 μm sections with a cryostat. Either mouse anti-rat CD45 monoclonal antibody (BD Biosciences) or rabbit anti-human VEGF polyclonal antibody (Santa Cruz Biotechnology, Santa Cruz, California, USA) was used as the primary antibody and the secondary antibody was anti-mouse or anti-rabbit polyvalent-peroxidase conjugate (Nichirei, Japan). Peroxidase activity was visualised with 3,3′-diaminobenzidine as a chromogen.

VEGF mRNA quantification

To elucidate the effects of MB on the expression of angiogenic growth factors, we investigated VEGF mRNA expression in the ischaemic hind limb by real time reverse transcription polymerase chain reaction (PCR). Changes in the amount of VEGF mRNA in the ischaemic muscle were quantified by reverse transcription PCR. The rats were killed at predetermined arbitrary time points after microbubble treatment with an overdose of sodium pentobarbital. The total RNA was extracted from ischaemic tissue samples and reverse transcribed with Ready-To-Go You-Prime First-Strand Beads (Amersham Biosciences). The synthesised cDNA was quantified by TaqMan quantitative PCR analysis of each gene with the ABI PRISM 7700 detection system (Applied Biosystems, Foster City, California, USA) according to the manufacturer's protocol.

Isolation of rat BM-MNCs

We examined the effect of microbubble treatment combined with BMT. Bone marrow was harvested by flushing the tibias and femurs of Lewis rats with Dulbecco's modified Eagle's medium supplemented with 10% fetal bovine medium. The plug of whole marrow cells was dispersed by passing it through pipettes of decreasing sizes. After a homogeneous cell suspension was achieved, mononuclear cells were isolated by density gradient centrifugation (Nyco Prep 1.077 Animal; Axis-Shield PoC AS, Oslo, Norway).

Combination of microbubble treatment and BMT

Additional rats (n = 21) were subjected to unilateral hind limb ischaemia and randomly divided into three groups. At day 7, the control group (n = 7) received 2.5 ml saline. The second group (n = 7) received BM-MNCs (5×10^6 cells/animal; BMT group) transplanted into the ischaemic thigh skeletal muscle with a 26 gauge needle at six different points. The third group (n = 7) received microbubble treatment followed by BMT (5×10^6 cells/animal; MB+BMT group). Laser Doppler and histological analyses were performed as described above.

Downloaded from heart.bmj.com on 29 March 2009

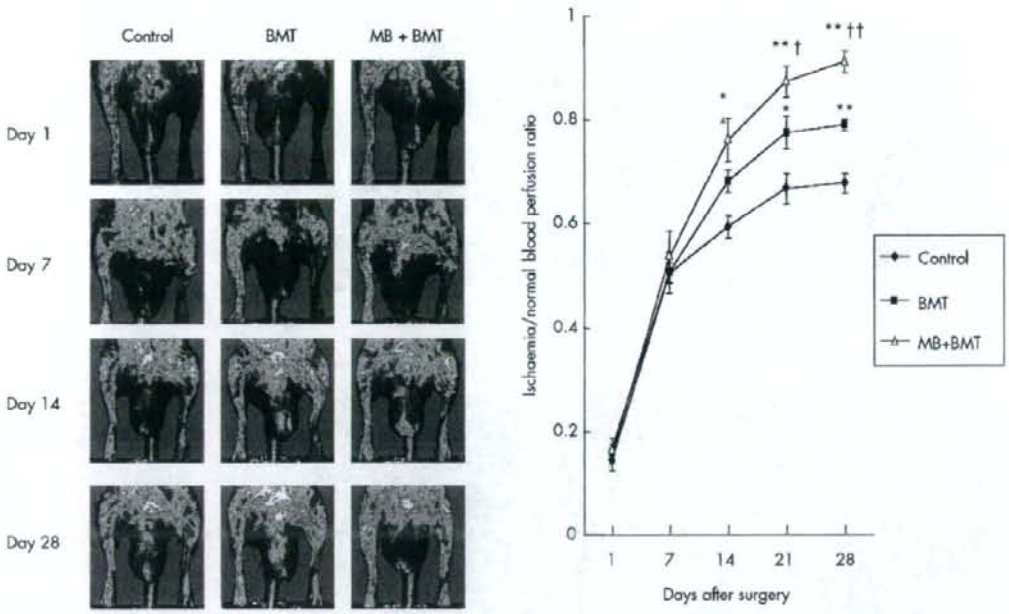

Figure 3 Representative LDBF images and line graph of calculated LDBFI. LDBFI increased significantly in the bone marrow mononuclear cell (BM-MNC) transplanted group (BMT) compared with control. The combination of microbubble treatment and BMT (MB+BMT) led to a significant further increase in LDBFI compared with BMT. *p < .05 v control; **p < 0.01 v control; †p < 0.05 v BMT; ††p < 0.01 v BMT.

Statistical analysis

Results were expressed as mean (SEM). Significance was determined by analysis of variance and the Student-Newman-Keuls test. Differences were considered significant at $p < 0.05$.

RESULTS

Neovascularisation by MB

To analyse subcutaneous blood flow, LDBF was analysed once weekly after hind limb ischaemia (fig 1A, B). An increase in LDBFI was observed in the ischaemic limb of the MB group (1.2-fold increase at day 28, $p < 0.05$) compared with the control group. No significant differences in LDBFI were observed between the ultrasound group and the control group. At postoperative day 28, all animals were subjected to iliac angiography. Figure 1C shows representative angiograms. Collateral vessels were observed in the MB group rather than in the control group and the ultrasound group. Quantitative analysis by angiographic scores showed a significantly greater number of collateral vessels in ischaemic tissue from the MB group (1.4-fold increase, $p < 0.01$) than from the control group. Ultrasound treatment alone did not change the angiographic score compared with vehicle treatment. The medial thigh muscles of the ischaemic limbs were histologically examined at day 30 as described above. Figure 1D shows representative photomicrographs of histological sections from ischaemic tissue. Alkaline phosphatase staining showed the presence of numerous capillary endothelial cells in the MB group but a lower number of capillary endothelial cells in the control group. The capillary to muscle fibre ratio was greater (1.4-fold, $p < 0.01$) in the MB group than the control group. In contrast, the ratio of the ultrasound group did not differ significantly from that of the control group. Thus, the ultrasound treatment alone did not affect ischaemic tissue, whereas MB induced angiogenesis in this rat hind limb ischaemic model.

Inflammatory responses and VEGF expression in ischaemic limbs after MB

CD45 immunostaining showed major infiltration of inflammatory leucocytes in the MB group (fig 2A). The number of CD45 positive leucocytes was higher in the MB group than in control (fig 2B). Immunohistochemical staining with anti-VEGF showed a higher level of VEGF expression in the perivascular tissues retrieved from microbubble treated rats than in controls at day 2 after treatment (fig 2C). Moreover, VEGF mRNA expression was significantly increased (3.0-fold, $p < 0.05$) at 24 hours after ultrasound–microbubble treatment compared with the level before treatment (fig 2D).

MB augments neovascularisation by transplanted BM-MNCs

We investigated the effects of ultrasound–microbubble treatment in combination with BMT on neovascularisation in hind limb ischaemia. Hind limb blood flow was serially examined by LDBF analysis once weekly after surgery (fig 3). The LDBFI was significantly increased in the BMT group compared with the control group at days 21 and 28. Combination treatment (MB+BMT) led to a significant further increase in the LDBFI compared with BMT monotherapy at days 21 and 28. Formation of collateral vessels was evaluated by angiography at postoperative day 28 (fig 4A, B). Monotherapy with BMT increased the angiographic scores significantly compared with control and MB+BMT improved the angiographic scores further. To further evaluate the effect of BMT and MB+BMT on neovascularisation, the ischaemic muscles were examined histologically at day 30 as described above (fig 4C, D). BMT significantly increased the capillary to muscle fibre ratio compared with control. Moreover,

Downloaded from heart.bmj.com on 29 March 2009

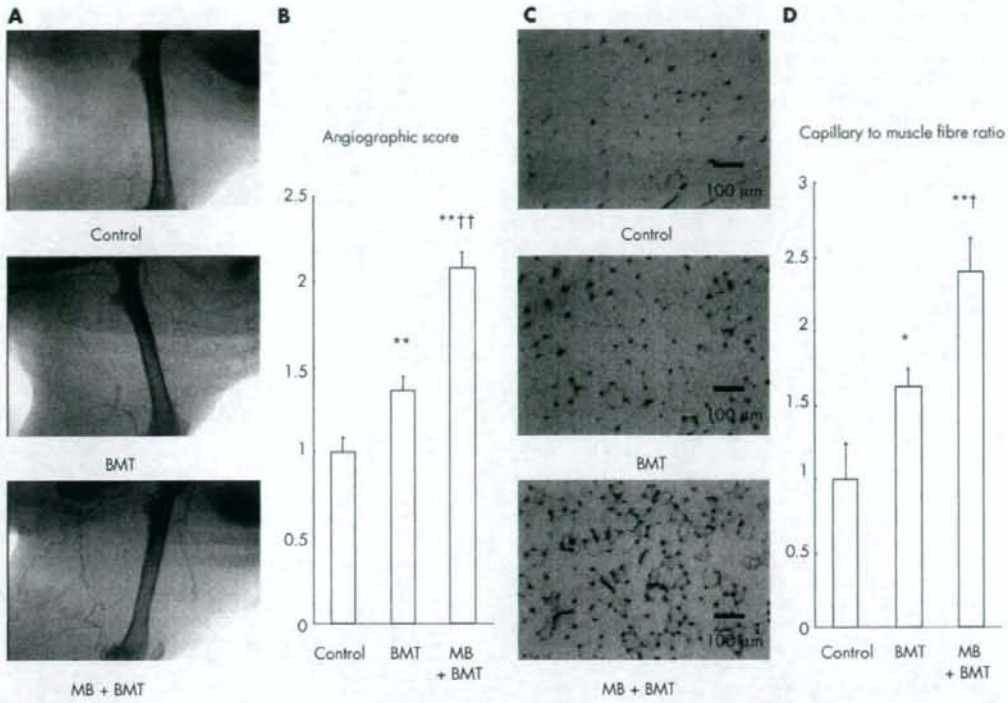

Figure 4 (A) Representative angiograms obtained on postoperative day 28. Numerous collateral vessels developed in the BMT and MB+BMT groups but not in controls. (B) Angiographic scores in ischaemic hind limbs were significantly higher after BMT than in controls. MB+BMT significantly further increased angiographic scores compared with BMT. **p < 0.01 v control; ††p < 0.01 v BMT. (C) Staining of ischaemic skeletal muscle tissues with alkaline phosphatase (dark blue) showing increased capillary count in the BMT and MB+BMT groups. (D) Quantitative analysis showed significantly higher capillary to muscle fibre ratios after BMT than in controls. MB+BMT led to a significant further increase in capillary to muscle fibre ratio compared with BMT. *p < 0.05 v control; **p < 0.01 v control; †p < 0.05 v BMT.

MB+BMT led to a further increase in capillary to muscle fibre ratio compared with BMT.

DISCUSSION

The major findings in the present study are, firstly, that MB induced neovascularisation in the ischaemic hind limb; and secondly, that ultrasound–microbubble treatment augmented neovascularisation by transplanted BM-MNCs in the ischaemic hind limb.

Although a previous study had suggested that inflammation created by the rupturing of capillaries initiates the arteriogenesis response,[5] the exact mechanism by which arteriogenesis is stimulated remains to be determined. Given the abundance of evidence that transmyocardial laser revascularisation induces neovascularisation through wound healing responses,[14 15] it is suggested that these small capillary ruptures may elicit neovascularisation through a similar mechanism. Recent studies have shown that transmyocardial revascularisation is associated with a significant angiogenic response, which appears to be mediated by the release of angiogenic growth factors such as VEGF, basic fibroblast growth factor, and transfoforming growth factor β.[16 17] In the present study, we observed that VEGF was upregulated after ultrasound–microbubble treatment in ischaemic muscle, suggesting a role for VEGF in ultrasound–microbubble treatment induced neovascularisation.

MB induces vascular injury. The repair of injury begins with the release of peptide growth factors from both inflammatory cells and injured cells as soon as tissue is damaged. Leucocytes affect many angiogenic processes, in part because leucocyte subtypes produce a large number of angiogenic factors, including VEGF, basic fibroblast growth factor, and various interleukins and proteinases (tryptase, chymase, matrix metalloproteinases, heparanase, and urokinase plasminogen activator).[18] Furthermore, Mohle *et al*[19] showed that thrombin activated platelets release VEGF and they suggested that VEGF delivered to sites of vascular injury by activated platelets may initiate angiogenesis. Taking together these results and our findings, it is reasonable to postulate that accumulation of blood cells after microbubble destruction elicits neovascularisation by supplying angiogenic factors.

Neovascularisation by VEGF in vivo[13] has been attributed to its mitogenic and promigratory effects on endothelial cells,[20 21] consistent with the concept that angiogenesis occurs by way of the development of sprouts from preexisting, fully differentiated endothelial cells. More recent studies have shown that VEGF contributes to postnatal neovascularisation by mobilising bone marrow derived EPCs.[22] It is suggested that VEGF may facilitate tissue neovascularisation, previously attributed exclusively to angiogenesis, in part by mobilising EPCs.

Downloaded from heart.bmj.com on 29 March 2009

Furthermore, direct effects of VEGF on transplanted BM-MNCs probably contributed to improved limb neovascularisation. VEGF is known to be essential for the in vitro differentiation of purified EPCs into mature endothelial cells.[25] This observation is consistent with in vivo studies showing the importance of VEGF for vasculogenesis.[26] Given that EPCs by definition express VEGF receptors, VEGF may also enhance EPC proliferation, adhesion, incorporation into endothelial cell monolayers, and differentiation to endothelial cells as reported previously.[24-26] These studies show the pivotal importance of VEGF and its receptors in blood vessel development. In the present study, BMT augmented angiogenesis and collateral vessel formation in ischaemic tissue. MB enhanced neovascularisation by transplanted BM-MNCs. In addition to the mechanical effects of capillary rupture by microbubble destruction, the augmentation may be partially due to VEGF expression after microbubble destruction. Altogether, local overexpression of VEGF and EPCs may promote neovascularisation in the target ischaemic tissues.

On the other hand, it has been reported that ultrasound can induce oxidative stress, endothelial cell damage, and increased microvascular permeability.[27 28] MB induced an inflammatory response causing local leucocyte infiltration, which may induce apoptosis and loss of cell membrane integrity.[29 30] Because the angiogenic effects may be related to tissue damage, further studies are needed to elucidate the clinical safety of this method.

In summary, our results show that MB can augment neovascularisation by transplanted BM-MNCs in the ischaemic hind limb. Microbubble treatment is likely to induce collateral vessel formation partly by supplying VEGF. The ultrasound-Optison method may be useful as a clinical intervention to enhance neovascularisation after BMT.

ACKNOWLEDGEMENTS

This work was supported by grants-in-aid (No 15590766 and 16590709) from the Ministry of Education, Science, and Culture. We thank Mihoko Watanabe and Azusa Inagaki for providing technical assistance.

Authors' affiliations

S Enomoto, M Yoshiyama, T Omura, R Matsumoto, T Kusuyama, D Nishiya, K Akioka, K Takeuchi, J Yoshikawa, Department of Internal Medicine and Cardiology, Osaka City University Medical School, Osaka, Japan

Y Izumi, H Iwao, Department of Pharmacology, Osaka City University Medical School, Osaka, Japan

REFERENCES

1 **Shohet RV**, Chen S, Zhou YT, *et al*. Echocardiographic destruction of albumin microbubbles directs gene delivery to the myocardium. *Circulation* 2000;**101**:2554–6.
2 **Price RJ**, Skyba DM, Kaul S, *et al*. Delivery of colloidal particles and red blood cells to tissue through microvessel ruptures created by targeted microbubble destruction with ultrasound. *Circulation* 1998;**98**:1264–7.
3 **Skyba DM**, Price RJ, Linka AZ, *et al*. Direct in vivo visualization of intravascular destruction of microbubbles by ultrasound and its local effects on tissue. *Circulation* 1998;**98**:290–3.
4 **Song J**, Chappell JC, Qi M, *et al*. Influence of injection site, microvascular pressure and ultrasound variables on microbubble-mediated delivery of microspheres to muscle. *J Am Coll Cardiol* 2002;**39**:726–31.
5 **Song J**, Qi M, Kaul S, *et al*. Stimulation of arteriogenesis in skeletal muscle by microbubble destruction with ultrasound. *Circulation* 2002;**106**:1550–5.
6 **Asahara T**, Murohara T, Sullivan A, *et al*. Isolation of putative progenitor endothelial cells for angiogenesis. *Science* 1997;**275**:964–7.
7 **Kamihata H**, Matsubara H, Nishiue T, *et al*. Implantation of bone marrow mononuclear cells into ischemic myocardium enhances collateral perfusion and regional function via side supply of angioblasts, angiogenic ligands, and cytokines. *Circulation* 2001;**104**:1046–52.
8 **Shintani S**, Murohara T, Ikeda H, *et al*. Augmentation of postnatal neovascularization with autologous bone marrow transplantation. *Circulation* 2001;**103**:897–903.
9 **Galmiche MC**, Koteliansky VE, Briere J, *et al*. Stromal cells from human long-term marrow cultures are mesenchymal cells that differentiate following a vascular smooth muscle differentiation pathway. *Blood* 1993;**82**:66–76.
10 **Kinnaird T**, Stabile E, Burnett MS, *et al*. Local delivery of marrow-derived stromal cells augments collateral perfusion through paracrine mechanisms. *Circulation* 2004;**109**:1543–9.
11 **Seifert FC**, Banker M, Lane B, *et al*. An evaluation of resting arterial ischemia models in the rat hind limb. *J Cardiovasc Surg (Torino)* 1985;**26**:502–8.
12 **Murohara T**, Asahara T, Silver M, *et al*. Nitric oxide synthase modulates angiogenesis in response to tissue ischemia. *J Clin Invest* 1998;**101**:2567–78.
13 **Takeshita S**, Zheng LP, Brogi E, *et al*. Therapeutic angiogenesis: a single intraarterial bolus of vascular endothelial growth factor augments revascularization in a rabbit ischemic hind limb model. *J Clin Invest* 1994;**93**:662–70.
14 **Bortone AS**, D'Agostino D, Schena S, *et al*. Inflammatory response and angiogenesis after percutaneous transmyocardial laser revascularization. *Ann Thorac Surg* 2000;**70**:1134–8.
15 **Malekan R**, Reynolds C, Narula N, *et al*. Angiogenesis in transmyocardial laser revascularization: a nonspecific response to injury. *Circulation* 1998;98: II62–5; discussion II66).
16 **Pelletier MP**, Glaid A, Sivaraman S, *et al*. Angiogenesis and growth factor expression in a model of transmyocardial revascularization. *Ann Thorac Surg* 1998;**66**:12–8.
17 **Horvath KA**, Chiu E, Maun DC, *et al*. Up-regulation of vascular endothelial growth factor mRNA and angiogenesis after transmyocardial laser revascularization. *Ann Thorac Surg* 1999;**68**:825–9.
18 **Norrby K**. Mast cells and angiogenesis. *Apmis* 2002;**110**:355–71.
19 **Mohle R**, Green D, Moore MA, *et al*. Constitutive production and thrombin-induced release of vascular endothelial growth factor by human megakaryocytes and platelets. *Proc Natl Acad Sci U S A* 1997;**94**:663–8.
20 **Leung DW**, Cachianes G, Kuang WJ, *et al*. Vascular endothelial growth factor is a secreted angiogenic mitogen. *Science* 1989;**246**:1306–9.
21 **Plouet J**, Schilling J, Gospodarowicz D. Isolation and characterization of a newly identified endothelial cell mitogen produced by AtT-20 cells. *Embo J* 1989;**8**:3801–6.
22 **Asahara T**, Takahashi T, Masuda H, *et al*. VEGF contributes to postnatal neovascularization by mobilizing bone marrow-derived endothelial progenitor cells. *Embo J* 1999;**18**:3964–72.
23 **Shi Q**, Rafii S, Wu MH, *et al*. Evidence for circulating bone marrow-derived endothelial cells. *Blood* 1998;**92**:362–7.
24 **Carmeliet P**, Ferreira V, Breier G, *et al*. Abnormal blood vessel development and lethality in embryos lacking a single VEGF allele. *Nature* 1996;**380**:435–9.
25 **Iwaguro H**, Yamaguchi J, Kalka C, *et al*. Endothelial progenitor cell vascular endothelial growth factor gene transfer for vascular regeneration. *Circulation* 2002;**105**:732–8.
26 **Fong GH**, Rossant J, Gertsenstein M, *et al*. Role of the Flt-1 receptor tyrosine kinase in regulating the assembly of vascular endothelium. *Nature* 1995;**376**:66–70.
27 **Basta G**, Venneri L, Lazzerini G, *et al*. In vitro modulation of intracellular oxidative stress of endothelial cells by diagnostic cardiac ultrasound. *Cardiovasc Res* 2003;**58**:156–61.
28 **Bertuglia S**, Giusti A, Picano E. Effects of diagnostic cardiac ultrasound on oxygen free radical production and microvascular perfusion during ischemia reperfusion. *Ultrasound Med Biol* 2004;**30**:549–57.
29 **Takeuchi H**, Ohmori K, Kondo I, *et al*. Interaction with leukocytes: phospholipid-stabilized versus albumin-shell microbubbles. *Radiology* 2004;**230**:735–42.
30 **Korosoglou G**, da Silva KG, Hansen A, *et al*. Ultrasound contrast agents can influence the respiratory burst activity of human neutrophil granulocytes. *Ultrasound Med Biol* 2004;**30**:75–81.

J Med Primatol doi:10.1111/j.1600-0684.2006.00192.x

ORIGINAL ARTICLE

Left ventricular volume and function in cynomolgus monkeys using real-time three-dimensional echocardiography

Hideshi Tsusaki[1], Haruno Yonamine[1], Asako Tamai[1], Mutsuko Shimomoto[2], Koichi Kuwano[1], Hiroshi Iwao[3], Ryoichi Nagata[1] & Go Kito[1]

1 Shin Nippon Biomedical Laboratories (SNBL) Ltd, Miyanoura, Kagoshima, Japan
2 Philips Medical Systems Corporation, Fukuoka, Japan
3 Department of Pharmacology, Osaka City University Medical School, Osaka, Japan

Keywords
β-blockers – cardiac function – ejection fraction – non-human primate – three-dimensional echocardiography

Correspondence
Hideshi Tsusaki, DVM, Shin Nippon Biomedical Laboratories Ltd, 2438 Miyanoura, Kagoshima 891-1394, Japan.
Tel.: 81 99 294 2600;
fax: 81 99 294 3619;
e-mail: tsusaki-hideshi@snbl.co.jp

Accepted August 2, 2006.

Abstract

Background The purpose of this study was to investigate the feasibility of evaluating cardiac function by real time three-dimensional (RT3D) echocardiography in isoflurane-anesthetized male cynomolgus monkeys. Additionally differences between inhibitory effects of β-blockers and a Ca channel blocker on left ventricular (LV) function were examined.
Methods and Results End-diastolic volume (EDV), end-systolic volume (ESV) and ejection fraction (EF) in the control (without any drug effect) were not significantly changed by repetitive measurement at a 30-day interval. Propranolol and metoprolol (0.1 and 0.3 mg/kg/10 minutes, i.v.) caused a dose-dependent increase in ESV, but little effect on EDV, resulting in a decrease in EF. Verapamil (0.1 and 0.3 mg/kg/10 minutes, i.v.) increased both EDV and ESV, but decreased EF was noted at 0.3 mg/kg.
Conclusions These results demonstrate the feasibility of RT3D echocardiography in providing reproducible estimations of LV volume and EF in monkeys when evaluating drugs that may affect cardiac function.

Introduction

Accurate quantification of left ventricular (LV) volume and function under non-invasive condition is important in decision-making in pre-clinical assessment, such as safety and pharmacology studies. LV volume and ejection fraction (EF) are particularly important indices for serial assessments of LV function in safety and pharmacology studies. Cardiac function measurements in anesthetized animals using devices such as the Swan–Ganz thermodilution catheter or Millar catheter can be used to assess LV function, but these are limited by their invasiveness or lack of repeatability. Two-dimension echocardiography has been a popular non-invasive modality for evaluating LV volume and EF in experimental studies; however, this method is limited by assumptions about LV cavity geometry which may not hold for patients with cardiomyopathy [6, 14]. Furthermore, treatment with certain drugs, including doxorubicin, produces significant changes in LV geometry, and the accuracy of LV volume measurements by two-dimensional methods might be compromised by assumptions on geometric shape [1, 2].

Recently, real-time three-dimensional (RT3D) echocardiography was introduced into clinical diagnosis, enabling accurate quantification of LV volume. In several recent studies, good results from RT3D echocardiography in determination of volume and left ventricle function have been reported [10–12, 14]. In brief, three separate steps are required to assess LV volume and function using RT3D echocardiography: (1) data acquisition by a full matrix array transducer, (2) image

processing at the endocardial border from multiple equi-angled longitudinal slices through the apex, and (3) data analysis with dedicated software [15]. Three-dimensional echocardiography is used in clinical diagnosis of morphological cardiac disease and it is reported that this technique could provide a significant tool for diagnosis and assessment of heart disease [5]. However, data from experimental studies using RT3D echocardiography are scarce.

Non-human primates are useful experimental animals for evaluating drug effects on the cardiovascular system, and are widely used in toxicological and pharmacological studies. In addition, it has been reported that the electrocardiography profile of freely moving conscious rhesus monkeys resembled that in humans [4]. Previously, we reported that RT3D echocardiography enables determination of not only 3D LV shape in motion but also LV volume and function in cynomolgus monkeys [16]. The purpose of this study was to investigate the feasibility of evaluating cardiac function and to examine any differences in inhibitory effects of β-blockers and a Ca channel blocker on LV function by using RT3D echocardiography in cynomolgus monkeys.

Materials and Methods

Animals

All procedures involving animals were approved by the Animal Care and Use Committee of Shin Nippon Biomedical Laboratories and were performed in accordance with standards published by the National Research Council (Guide for the Care and Use of Laboratory Animals, NIH OACU), the National Institutes of Health Policy on Human Care and Use of Laboratory Animals. In accordance with these standards, every effort was made to ensure that the subjects were free of pain and discomfort. The principal investigator and the primate handling staff were present for all procedures.

Nineteen male cynomolgus monkeys (*Macaca fascicularis*, purpose-bred) aged 4–5 years, imported from China, were used in this study. After 1-month regulatory quarantine, the animals were acclimated in the test facility stock colony until use. The animals were housed singly in stainless-steel cages [68 cm (D) × 62 cm (W) × 77 cm (H)] in a test room maintained at a temperature of 26 ± 2°C and 50 ± 10% humidity with artificial lighting from 06:00 to 18:00 hours and with air changes 15 times per hour. They were fed Teklad Global 25% Protein Primate Diet (Harlan Sprague Dawley, Inc., Indianapolis, IN, USA) and water (on-site well) was provided *ad libitum*. On the days when experiments were conducted, the animals weighed between 4.0 and 5.2 kg.

Echocardiographic examination

The animals were restrained in a restrainer designed in-house (US patent no. 5571241), and anesthesia was then induced via a mask made from a plastic bottle containing cotton soaked in isoflurane (Abbott Laboratories, Abbott Park, IL, USA) at its base. After transfer to the experimental room, the animals were intubated with a 3.0 mm endotracheal tube (107–030; Mallinckrodt Medical Ltd, Hazelwood, MO, USA) for maintenance of anesthesia, and restrained in the left lateral position under a closed isoflurane inhalation anesthesia system. Heart rate (HR) was maintained at 130 ± 10 beats/minute, and the isoflurane concentration at 1.5–2.0%. Blood pressure and expired CO_2 concentration were continuously monitored (BSM-2391; Nihon Kohden, Tokyo, Japan) during the experimental period. RT3D echocardiography was performed with a Philips Medical echocardiography system (SONOS 7500; Philips Medical Systems, Andover, MA, USA). In this study, the apical window was used to obtain RT3D echocardiography images for LV volume measurement. This unit used a full matrix-array transducer (x4; Philips Medical Systems) for rapid beam forming to scan a pyramidal volume. Real-time volumetric scanning required no off-line reconstruction techniques, enabling dynamic three-dimensional visualization and quantification of the heart in real time using a transthoracic approach. Images were viewed in a 'live 3D' or 'full volume' mode.

RT 3D echocardiography data reconstruction and analysis

One full volume acquisition took 5–8 s. The pyramidal dataset obtained from the apical four-chamber view contained the whole heart structure. Data analysis was performed using the TomTec 4D Cardio-View RT (TomTec GMBH, Unterschleissheim, Germany). Eight longitudinal levels at intervals of 22.5° were selected around this rotation axis. End-diastolic and end-systolic volumes (EDV and ESV), calculated with the TomTec 4D Cardio-View RT. The following parameters were manually calculated;

$$\text{Stroke volume} : SV = EDV - ESV$$

$$\text{LV ejection fraction} : EF = SV/EDV \times 100$$

$$\text{Cardiac output} : CO = SV \times HR$$

J Med Primatol 36 (2007) 39–46 © 2006 The Authors
Journal compilation © 2006 Blackwell Munksgaard

Echocardiographic parameters

For acquisition of basal echocardiographic parameters, six naïve (drug free) animals were used. An additional six animals were used for repetitive measurements. The day on which echocardiography was initiated was designated as Day 1. Echocardiography was also conducted on 7th and 30th day. Animals received drugs during the intervals between measurements; however, measurements were not conducted until at least 3 days after the most recent drug treatment.

Effects of drugs

Thirteen animals were used for drug treatment studies, and where applicable, the interval between drug treatments was at least 3 days. After baseline echocardiographic parameters for each animal were determined, each drug was intravenously infused for 10 minutes. Echocardiographic parameters were recorded 10 minutes after starting infusion (at termination of drug infusion), and 30 minutes after the end of infusion. For intravenous administration, propranolol (FK270, AstraZeneca, K.K., Osaka, Japan, and FH269; Sumitomo Pharmaceuticals Co. Ltd), verapamil (56H0925; Sigma-Aldrich, St Louis, MO, USA) and metoprolol (101K1517; Sigma-Aldrich) were dissolved in saline at a concentration of 1 or 3 mg/ml. The infusion rate of each drug was 0.1 ml/kg/minute. The drug dosages were set at 0.1 and 0.3 mg/kg, approximating the clinical dose (5 mg per man) and slightly higher than the clinical dose, respectively [7].

Statistical analysis

The results are expressed as mean ± SD and are accompanied by the number of observations. Statistical analysis of the data between pre-drug values and post-drug values was conducted by paired t-test. Differences of $P < 0.05$ were considered statistically significant.

Results

Echocardiographic parameters

Table 1 shows basal parameters of LV and cardiovascular function, including EDV, ESV, EF, SV, CO, and HR from naïve (drug free) animals. EF values, which are one of the most important parameters for evaluation of LV function, were very similar among the animals. Table 2 shows repetitive measurements of EDV, ESV, EF, SV, CO and HR over a 30-day period. Each parameter in individual animals showed a steady value over a prolonged period.

Effect of drugs

Effects of propranolol, metoprolol and verapamil are shown in Tables 3, 4 and 5, respectively. There were no differences in LV function parameters (EDV, ESV, EF, SV and CO) before administration of each drug (propranolol, metoprolol and verapamil).

Propranolol

Propranolol at 0.1 and 0.3 mg/kg caused 18–23% decrease in HR at the end of intravenous infusion. Propranolol had no effect on blood pressure. As shown in Fig. 1 (left column), propranolol (0.1 and 0.3 mg/kg/10 minutes, each n = 5) caused a significantly marked increase (52.2%) in ESV. EDV was slightly, but not significantly, increased at both dose levels. These changes resulted in a decrease in EF and SV. Furthermore, CO markedly decreased by as much as 40%, concomitant with decreased HR. These effects could still be observed 30 minutes after the end of infusion.

Metoprolol

Metoprolol at 0.1 (n = 3) and 0.3 mg/kg also caused 20–28% decrease in HR at the end of infusion.

Table 1 Basal echocardiographic parameters of left ventricular function in anesthetized cynomolgus monkey

Animal no.	EDV (ml)	ESV (ml)	EF (%)	SV (ml)	CO (ml/minute)	HR (beats/minute)
1	4.4	2.1	53.4	2.3	308.2	134.0
2	7.2	3.3	54.9	3.9	503.1	129.0
3	4.8	2.1	56.8	2.7	326.7	121.0
4	5.3	2.3	56.9	3.0	390.0	130.0
5	4.8	2.1	55.9	2.7	313.2	116.0
6	6.9	3.1	55.0	3.8	501.6	132.0
Mean	5.6	2.5	55.5	3.1	390.5	127.0
SD	1.2	0.6	1.3	0.6	91.5	7.0

EDV, end-diastolic volume; ESV, end-systolic volume; EF, ejection fraction; SV, stroke volume; CO, cardiac output; HR, heart rate.

Table 2 Echocardiographic parameters of left ventricular function obtained by repetitive measurements (on the 7th and 30th day) in the same monkeys

Number of measurement	Animal no.	EDV (ml)	ESV (ml)	EF (%)	SV (ml)	CO (ml/minute)	HR (beats/minute)
1	7	4.8	2.0	58.9	2.8	344.4	123
	8	4.1	1.8	56.9	2.3	276.0	120
	9	4.6	1.9	58.8	2.7	334.8	124
	10	5.4	2.4	55.9	3.0	357.0	121
	11	4.3	1.9	56.4	2.5	286.7	117
	12	5.0	2.1	58.0	2.9	368.3	127
	Mean	4.7	2.0	57.5	2.7	327.9	122.0
	SD	0.5	0.2	1.3	0.3	37.9	3.5
2 (7th day)	7	5.0	2.1	58.3	2.9	353.8	122
	8	3.9	1.6	58.1	2.3	280.6	122
	9	4.3	1.8	58.5	2.5	335.0	134
	10	5.8	2.2	62.6	3.6	500.4	139
	11	4.1	1.7	58.1	2.4	317.3	135
	12	5.1	2.2	55.6	2.9	347.7	122
	Mean	4.7	1.9	58.5	2.8	355.8	129.0
	SD	0.7	0.3	2.3	0.5	75.6	7.8
3 (30th day)	7	5.0	2.1	58.3	2.9	353.8	122
	8	4.1	1.8	57.2	2.4	310.2	132
	9	4.3	1.8	58.6	2.6	359.6	141
	10	6.0	2.4	61.3	3.7	489.1	134
	11	4.0	1.6	60.1	2.5	325.9	133
	12	5.1	2.2	57.6	2.9	359.6	124
	Mean	4.7	1.9	58.8	2.8	366.4	131.0
	SD	0.8	0.3	1.6	0.5	63.4	7.0

The day in parenthesis showed the days from the first measurement.
EDV, end-diastolic volume; ESV, end-systolic volume; EF, ejection fraction; SV, stroke volume; CO, cardiac output; HR, heart rate.

Table 3 Effects of propranolol on left ventricular function in cynomolgus monkeys using RT 3D echocardiographic technique

Propranolol (mg/kg/10 minutes)	EDV (ml)	ESV (ml)	EF (%)	SV (ml)	CO (ml/minute)	HR (beats/minute)
0.1 (n = 5)						
Pre-drug	4.9 ± 0.7	2.0 ± 0.2	59.0 ± 2.4	2.9 ± 0.5	375 ± 80.0	127.2 ± 7.2
10 minutes	4.9 ± 0.7	2.6 ± 0.4**	46.9 ± 2.2***	2.3 ± 0.3**	237 ± 29.3**	103.0 ± 3.9**
30 minutes	5.0 ± 0.7	2.7 ± 0.4*	46.4 ± 1.9**	2.3 ± 0.3**	231 ± 22.6**	101.0 ± 7.8**
0.3 (n = 5)						
Pre-drug	4.9 ± 0.8	2.0 ± 0.3	58.5 ± 1.6	2.9 ± 0.5	376 ± 69.8	127.2 ± 7.2
10 minutes	5.4 ± 1.1	3.1 ± 0.7**	42.1 ± 3.1 **	2.3 ± 0.5*	226 ± 48.7**	103.0 ± 3.9**
30 minutes	5.5 ± 1.1	3.0 ± 0.8*	45.9 ± 4.4**	2.5 ± 0.3*	237 ± 36.6**	101.0 ± 7.8**

Date are expressed as the mean ± S.D. Propranolol was intravenously infused for 10 minutes.
EDV, end-diastolic volume; ESV, end-systolic volume; EF, ejection fraction; SV, stroke volume; CO, cardiac output; HR, heart rate.
Significantly different from pre-valve, at $*P < 0.05$, $**P < 0.01$ and $***P < 0.001$, respectively.

Metoprolol (0.3 mg/kg/10 minutes, n = 4) produced a significant increase in ESV (46.8%), but EDV was not significantly changed. These changes resulted in a decrease in EF, SV and CO (Fig. 1 middle column). The inhibitory effect of metoprolol persisted for about 30 minutes.

Verapamil

Verapamil produced a decrease in HR by about 10%, but had no effect on blood pressure. Verapamil (0.1 mg/kg/10 minutes, n = 5) produced significant increases both in EDV and ESV, and thereby SV and CO maintained almost pre-values despite a very slight decrease in EF (Fig. 1 right column). At a dose of 0.3 mg/kg (n = 5), EDV and ESV increased by 17% and 47%, respectively. However, a maintenance rate of about 80% in EF and CO was obtained even at the end of intravenous infusion. Dynamic casts of LV during EDV (diastolic phase) and ESV (systolic phase) before and after intravenous infusion of verapamil (0.3 mg/kg/10 minutes) are shown in Fig. 2.

J Med Primatol 36 (2007) 39–46 © 2006 The Authors
Journal compilation © 2006 Blackwell Munksgaard

Table 4 Effects of metoprolol on left ventricular function in cynomolgus monkeys using RT 3D echocardiographic technique

Metoprolol (mg/kg/l0 minutes)	EDV (ml)	ESV (ml)	EF (%)	SV (ml)	CO (ml/minute)	HR (beats/minute)
0.1 (n = 3)						
Pre-drug	4.8 ± 0.5	2.0 ± 0.2	58.2 ± 2.0	2.8 ± 0.3	374 ± 76.6	132.0 ± 13.1
10 minutes	4.8 ± 0.6	2.5 ± 0.2 *	47.1 ± 1.2**	2.3 ± 0.4**	239 ± 42.8	105.7 ± 10.1
30 minutes	5.1 ± 0.3	2.4 ± 0.3 *	52.2 ± 2.2	2.7 ± 0.1	286 ± 11.3	107.3 ± 4.9
0.3 (n = 4)						
Pre-drug	4.7 ± 1.0	1.9 ± 0.3	58.2 ± 4.0	2.8 ± 0.7	379 ± 114.9	136.0 ± 6.4
10 minutes	5.1 ± 0.7	2.8 ± 0.3**	44.4 ± 5.1**	2.3 ± 0.6*	217 ± 37.4 *	96.5 ± 12.1*
30 minutes	5.1 ± 0.6	2.6 ± 0.2 *	49.6 ± 3.4*	2.6 ± 0.5	249 ± 27.9	98.3 ± 12.7*

Date are expressed as the mean ± SD. Metoprolol was intravenously infused for 10 minutes.
EDV, end-diastolic volume; ESV, end-systolic volume; EF, ejection fraction; SV, stroke volume; CO, cardiac output; HR, heart rate.
Significantly different from pre-valve, at $*P < 0.05$ and $**P < 0.01$, respectively.

Table 5 Effects of verapamil on left ventricular function in cynomolgus monkeys using RT 3D echocardiographic technique

Verapamil (mg/kg/10 minutes)	EDV (ml)	ESV (ml)	EF (%)	SV (ml)	CO (ml/minute)	HR (beat/minute)
0.1 (n = 5)						
Pre-drug	4.9 ± 1.1	2.1 ± 0.5	58.1 ± 1.5	2.8 ± 0.6	374 ± 93.3	131 ± 8.0
10 minutes	5.5 ± 1.1**	2.7 ± 0.7**	52.4 ± 2.6**	2.9 ± 0.4	357 ± 42.1	125 ± 9.6
30 minutes	5.2 ± 1.2	2.5 ± 0.7	53.0 ± 3.2	2.7 ± 0.5	325 ± 54.6	119 ± 9.2
0.3 (n = 5)						
Pre-drug	4.5 ± 0.5	1.9 ± 0.3	57.1 ± 2.0	2.6 ± 0.3	343 ± 31.7	134 ± 6.5
10 minutes	5.2 ± 0.9**	2.8 ± 0.5**	45.8 ± 1.5***	2.4 ± 0.4	279 ± 57.2*	116 ± 10.3
30 minutes	5.0 ± 0.7*	2.7 ± 0.6**	45.6 ± 4.7**	2.3 ± 0.3	268 ± 48.9*	116 ± 6.2*

Date are expressed as the mean ± SD. Verapamil was intravenously infused for 10 minutes.
EDV, end-diastolic volume; ESV, end-systolic volume; EF, ejection fraction; SV, stroke volume; CO, cardiac output; HR, heart rate.
Significantly different from pre-valve, at $*P < 0.05$, $**P < 0.01$ and $***P < 0.001$, respectively.

Discussion

The purpose of this study was to investigate the feasibility of assessing cardiac function in anesthetized monkeys. Using RT3D echocardiography, data on LV function parameters, including EDV, ESV, SV, EF and CO were collected. EDV and ESV in cynomolgus monkey showed unexpectedly low values ranging from 2 to 6 ml. We have previously stated that the minimum mass that can be measured by RT3D echocardiography ranges from 1.5 to 1.9 ml, that is, the accuracy of volume measurements obtained from RT3D echocardiography [16]. In safety and pharmacological studies using large experimental animals, drug effects are frequently evaluated by comparison of pre- and post-dose results. Therefore, the reproducibility of results is important in the interpretation of drug effects. In the present study, EDV and ESV showed steady values in repetitive measurements of the same cynomolgus monkeys by RT3D echocardiography, suggesting that this technique can be applied to safety and pharmacological studies over a prolonged period.

We reported that although there was a correlation between EDV calculated from 2D echocardiography and that calculated from RT3D echocardiography, and that LV volumes obtained by 2D echocardiography were greater than those obtained with RT3D echocardiography [16]. Specifically, overestimation of LV volume measured in cynomolgus monkeys by 2D echocardiography must be taken into account. However, Handke *et al.* [3] reported that the difference in cardiac output between RT3D echocardiography and thermodilution is due primarily to overestimation by thermodilution. Cardiac output estimated by thermodilution is calculated from blood flow, and that estimated by RT3D echocardiography from LV volume and HR. RT3D echocardiography as a direct method of measuring cardiac output shows greater precision and reproducibility than thermodilution [9]. Furthermore, conventional thermodilution techniques require invasive pulmonary artery catheters, which may excessively burden the heart of the cynomolgus monkey, as this species is relatively small compared with other large experimental animals, such as the dog. In light of these

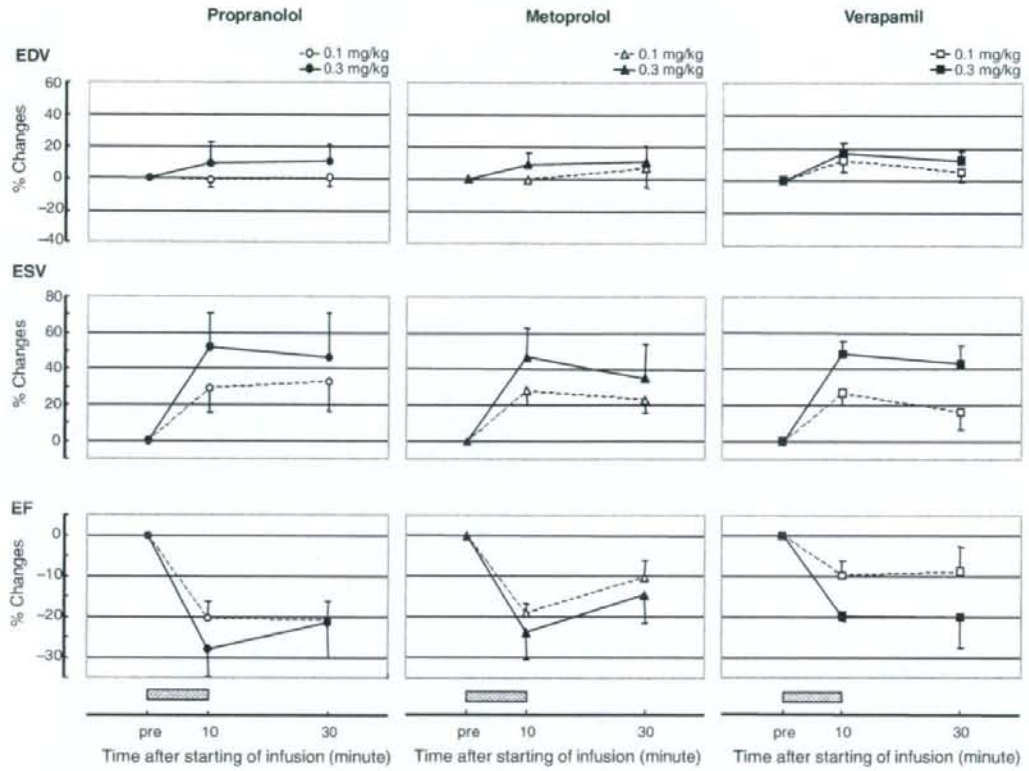

Fig. 1 Effects of propranolol, metoprolol and verapamil on end-diastolic volume, end-systolic volume, and ejection fraction in anesthetized monkeys. Propranolol (0.1 and 0.3 mg/kg/10 minutes), metoprolol (0.1 and 0.3 mg/kg/10 minutes) and verapamil (0.1 and 0.3 mg/kg/10 minutes) were infused at a rate of 0.1 ml/kg/minute for 10 minutes (expressed as column on the abscissa axis). The data show the changes in the measured variables expressed as percentage of initial value. Each point represents the mean ± SD from three to five monkeys.

factors, RT3D echocardiography may have considerable potential for assessment of LV function in monkeys in various preclinical studies.

We also investigated the effect of β-blockers for evaluation of cardiac function by RT3D echocardiography in cynomolgus monkeys. We found from RT3D echocardiography that the inhibitory effects of β-blockers and those of verapamil on LV function differ between individual healthy cynomolgus monkeys. The inhibitory effects of propranolol and metoprolol on LV function were represented by intensive depression of cardiac contractility, shown as an increase in ESV, namely negative inotropic action, resulting in severe decreases in EF and CO even at a low dose (0.1 mg/kg/10 minutes). This is a widely recognized effect of β-blockers in the heart. It is reported that decreases in CO and SV by β-blockers are slight even though β-blockers reduce HR and increase EDV [18]. Our data also showed that depression of cardiac function, particularly CO, by propranolol and metoprolol in the healthy heart is accompanied by a marked reduction in HR. Moreover, both propranolol and metoprolol barely increased EDV, and showed little dilating action on LV, even at a high dose (0.3 mg/kg/10 minutes).

β-Blockade is one of the most effective treatments for heart failure. However, it might appear counterintuitive to use β-blockers for the treatment of heart failure, because they are known to acutely decrease contractility in healthy hearts [7]. It is reasonable, therefore, that treatment with β-blockers should be initiated under careful observation, using a gradually increasing low dose. However, β-blockers are recognized as an integral part of therapy for heart failure

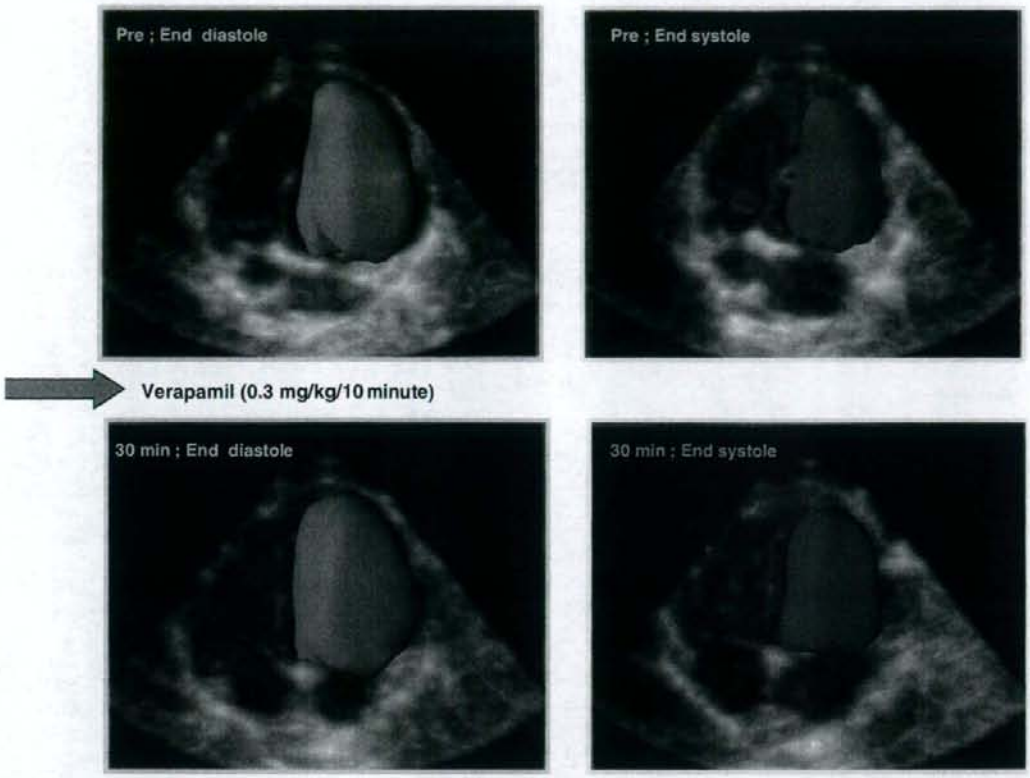

Fig. 2 Dynamic casts of LV at end diastolic and end systolic phases before and after intravenous infusion of verapamil (0.3 mg/kg/10 minutes). The 3D volume data set was automatically divided into a number (n = 8) of predetermined equi-angled longitudinal slices through the apex. In each of the longitudinal slices an automated border detection algorithm was then used to track endocardial borders throughout the cardiac cycle to obtain a dynamic cast of the LV.

based on principles of antagonism of the neurohumoral response [8, 13].

Data from treatment with verapamil, a Ca channel blocker, showed depression of cardiac contraction was concomitant with slight LV dilation, and EF maintained > 50% at a low dose level (0.1 mg/kg/10 minutes), although it was statistically significant. It is accepted that preserved LV function is EF > 50% in human [17], and this decreased EF at a low dose level of verapamil is judged to be of no biological significance. Verapamil produced dose-dependent increases in EDV and ESV. The increase in ESV was similar to that from propranolol; however, verapamil significantly increased EDV in comparison with propranolol. Thereby, SV and CO maintained almost pre-dose values. Furthermore, it is of special importance in the therapy of ischemic heart disease that the high maintenance rate of about 80% in CO was obtained even at a high dose, because verapamil has little negative chronotropic action.

In the present study, we demonstrate for the first time that β-blockers including propranolol and metoprolol do not increase EDV in the healthy heart, namely, having no effect on dilation action on LV function. This finding may explain the main difference in inhibitory effects between β-blockers and verapamil in the healthy heart, resulting in a marked inhibitory action of β-blockers in comparison with verapamil. It may be difficult to detect these differences by change in LV pressure for measurement of LV function, whereas accurate quantification of LV volume by RT3D echocardiography is clearly superior in comparison with conventional methods.

In conclusion, RT3D echocardiography provides reproducible and repeatable data on cardiac LV

volume and function in cynomolgus monkeys. It was of interest that β-blockers including propranolol and metoprolol produced a more increase in ESV than EDV, resulting in a reduction in EF in healthy hearts of cynomolgus monkeys, and verapamil produced increases in both ESV and EDV at low dose, and maintained EF. These results demonstrate that RT3D echocardiography provides a feasible and accurate estimation of LV volume and EF in cynomolgus monkeys. Furthermore, we confirmed that RT3D echocardiography allows a better evaluation of β-blockers and Ca channel blockers including propranolol and verapamil on LV volume and EF.

References

1. Christiansen S, Stypmann JJ, Jahn UR, Redmann K, Fobker M, Gruber AD, Scheld HH, Hammel D: Partial left ventriculectomy in modified adriamycin-induced cardiomyopathy in the dog. *J Heart Lung Transplant* 2003; **22**:301–8.
2. Hanai K, Takaba K, Manabe S, Nakano M, Kohda A, Matsuo M: Evaluation of cardiac function by echocardiography in dogs treated with doxorubicin. *J Toxicol Sci* 1996; **21**:1–10.
3. Handke M, Heinrichs G, Magosaki E, Lutter G, Bode C, Geibel A: Three-dimensional echocardiographic determination of cardiac output at rest and under dobutamine stress: Comparison with thermodilution measurements in the ischemic pig model. *Echocardiography* 2003; **20**:47–55.
4. Hassimoto M, Harada T, Kaga N, Murano H, Obata M: Accurate evaluation of QT interval in conscious rhesus monkeys (*Macaca mulatta*) by use of Holter ECG. *J Electrocardiol* 2002; **35**:333–42.
5. Lange A, Palka P, Burstow DJ, Godman MJ: Three-dimensional echocardiography: Historical development and current applications. *J Am Soc Echocardiogr* 2001; **14**:403–12.
6. Mitchell GF, Lamas GA, Vaughan DE, Pfeffer MA: Left ventricular remodeling in the year after first anterior myocardial infarction: a quantitative analysis of contractile segment lengths and ventricular shape. *J Am Coll Cardiol* 1992; **19**:1136–44.
7. Opie LH, Yusuf S: Beta-blocking agents. In: *Drugs for the Heart*, 5th edn. Opie LH (eds). Philadelphia: WB Saunders Company, 2001; 1–32.
8. Packer M, Cohn JN: Consensus recommendations for the management of chronic heart failure. *Am J Cardiol* 1999; **83**:1A–38A.
9. Pemberton J, Li X, Karamlou T, Sandquist CA, Thiele K, Shen I, Ungerleider RM, Kenny A, Sahn DJ: The use of live three-dimensional Doppler echocardiography in the measurement of cardiac output. *J Am Coll Cardiol* 2005; **45**:433–8.
10. Qin JX, Shiota T, Thomas JD: Determination of left ventricular volume, ejection fraction, and myocardial mass by real-time three-dimensional echocardiography. *Echocardiography* 2000; **17**:781–6.
11. Schmidt MA, Ohazama CJ, Agyeman KO, Freidlin RZ, Jones M, Laurienzo JM, Brenneman CL, Arai AE, von Ramm OT, Panza JA: Real-time three-dimensional echocardiography for measurement of left ventricular volumes. *Am J Cardiol* 1999; **84**:1434–9.
12. Schmidt MA, Freidlin RZ, Ohazama CJ, Jones M, Laurienzo JM, Brenneman CL, Norman JE, von Ramm OT, Panza JA: Anatomic validation of a novel method for left ventricular volume and mass measurements with use of real-time 3-dimensional echocardiography. *J Am Soc Echocardiogr* 2001; **14**:1–10.
13. Schrier RW, Abraham WT: Hormones and hemodynamics in heart failure. *N Engl J Med* 1999; **341**:577–85.
14. Shiota T, McCarthy PM, White RD, Qin JX, Greenberg NL, Flamm SD, Wong J, Thomas JD: Initial clinical experience of real-time three-dimensional echocardiography in patients with ischemic and idiopathic dilated cardiomyopathy. *Am J Cardiol* 1999; **84**:1068–73.
15. Sugeng L, Weinert L, Lang RM: Left ventricular assessment using real time three dimensional echocardiography. *Heart* 2003; **89**(Suppl. III):iii29–36.
16. Tsusaki H, Yonamine H, Tamai A, Shimomoto M, Iwao H, Nagata R, Kito G: Evaluation of cardiac function in primates using real-time three-dimensional echocardiography as applications to safety assessment. *J Pharmacol Toxicol Methods* 2005; **52**:182–7.
17. Tsutsui H, Tsuchihashi M, Takeshita A: Mortality and readmission of hospitalized patients with congestive heart failure and preserved versus depressed systolic function. *Am J Cardiol* 2001; **88**:530–3.
18. Yoerger DM, Weyman AE: Hypertrophic obstructive cardiomyopathy: Mechanism of obstruction and response to therapy. *Rev Cardiovasc Med* 2003; **4**: 199–15.

J Med Primatol **36** (2007) 39–46 © 2006 The Authors
Journal compilation © 2006 Blackwell Munksgaard

J Pharmacol Sci 107, 15 – 19 (2008)

Journal of Pharmacological Sciences
©2008 The Japanese Pharmacological Society

Forum Minireview

Pharmacogenomics of Cardiovascular Pharmacology: Molecular Network Analysis in Pleiotropic Effects of Statin — an Experimental Elucidation of the Pharmacologic Action From Protein-Protein Interaction Analysis

Masayuki Shiota[1,*], Hiromi Kusakabe[1], Yuko Hikita[1], Takafumi Nakao[1], Yasukatsu Izumi[1], and Hiroshi Iwao[1]

[1]*Department of Pharmacology, Osaka City University Medical School, 1-4-3 Asahimachi, Abeno-ku, Osaka 545-8585, Japan*

Received February 13, 2008; Accepted March 14, 2008

Abstract. The ebb and flow of cellular life depends largely on signaling pathways and networks, which are regulated by specific protein-protein interactions. These interactions often involve assembly of large signaling complexes containing many different protein kinases, protein phosphatases, their substrates, and scaffold proteins. Identification of protein complexes is the key to understanding cellular functions. One of the techniques used for the isolation of protein complexes is the affinity purification system. Inhibitors of 3-hydroxyl-3-methyglutaryl coenzyme A (HMG-CoA) reductase (i.e., statins) exert cholesterol-independent vasoprotective effects that are mediated, in part, through the activation of Akt. However, the molecular mechanism remains unknown. To elucidate the molecular mechanisms of the pleioptropic effects of statins, we searched for the binding molecule of Akt1 by using a combined mass spectrometry and affinity purification strategy. By this technique, we identified the protein-protein interactions of 23 proteins from statin-treated rat aortic endothelial cells (rAECs). Our results suggest that this approach is very effective and statin activates many Akt down-stream targets, not only endothelial nitric oxide synthase (eNOS). The methodology presented here would provide a new tool for chemical proteomics in medicinal science.

Keywords: network analysis, interaction, statin, pleiotropic effect, Akt, pharmacogenomics

1. Introduction

Numerous human diseases can be attributed to defects in cellular signal transduction pathways, which are regulated by specific protein-protein interactions. These interactions often involve assembly of large signaling complexes containing many different protein kinases, protein phosphatases, their substrates, and scaffold proteins. Therefore, identification of protein complexes is the key to understanding the physiological functions and molecular mechanisms of disease. A number of ongoing proteomics projects seek to define critical components of signal transduction networks. This type of study enables more intelligent design of therapeutic agents that can specifically correct disease-specific signaling alterations by targeting individual proteins. However, the identification of a protein complex remains a significant challenge because many interactions are transient in nature and the components that form these unstable complexes can be lost during sample preparation. Furthermore, it is also difficult to purify native protein complexes because many of them are expressed at low levels and might not possess a unique physical characteristic that permits their isolation or enrichment from a cell lysate. Therefore, a specific, simple method is necessary to clarify a signal network efficiently. Affinity purification and mass spectrometry (MS)-based protein identification is a powerful and highly sensitive technique for identifying protein-protein interactions and elucidating components of multiprotein complexes. This method can become one of these breakthroughs.

The 3-hydroxyl-3-methylglutaryl-coenzyme A (HMG-CoA) reductase inhibitors referred to as statins are

*Corresponding author. sio@med.osaka-cu.ac.jp
Published online in J-STAGE
doi: 10.1254/jphs.08R01FM